Nanopatterning of Anionic Nanoparticles based on Magnetic Prussian-Blue Analogues

Eugenio Coronado, Alicia Forment-Aliaga,* Elena Pinilla-Cienfuegos, Sergio Tatay, Laure Catala, and José A. Plaza*

Prussian-blue analogues (PBA) are a family of molecule-based magnetic compounds of general formula $A_xM_y[M'(CN)_6]_z$, whose magnetic properties can be tuned by an external stimulus. This tunability makes PBA good candidates for their integration into new electronic or spintronic devices. As a previous step to accomplish this integration, PBA need to be deposited onto surfaces in controllable ways and if possible into specific positions on the surface. Even though the study of PBA has traditionally been limited to bulk, lately they have also been processed as nanoparticles (NPs). Here an efficient approach is presented for the accurate deposition and organization of PBA-NPs of different sizes (from ~6 to ~25 nm) over silicon surfaces. The approach used in this work, relies on a combination of surface functionalization with local oxidation nanolithography (LON) and uses electrostatic interactions between PBA-NPs and a charged self-assembled monolayer patterned on specific parts of the silicon surface. By using atomic force microscopy (AFM), magnetometry, infrared spectroscopy (IR) and auger electron spectroscopy (AES) we show that the deposition process does not affect NPs properties. In addition, we present a study on the evolution of AFM nanolithographed SiO_2 patterns under sonication.

1. Introduction

A key requirement to incorporate functional nano-objects as nanoscale elements for devices is the positioning of these objects on a surface with nanoscale accuracy. With this aim, new methods have been developed, as the one proposed by Cavallini et al. based on the integration of nanoparticles into patterned silicon oxide features by applying a voltage between a stamp and a silicon surface with the solution containing the nanoparticles in between.[1] In this context, a combination of self-assembly "bottom-up" approaches with "top-down" lithographic techniques has shown to be very suitable to selectively deposit molecular objects onto the nanopatterns fabricated from local oxidation nanolithography.[2–5] The method is based on the electrostatic interactions established between a self-assembled monolayer (SAM) of aminopropyltriethoxysilane (APTES) located on SiO_2 marks and negatively charged nanoparticles. The method is quite general and has already been used for the positioning of any kind of charged nanoparticle[5] (either cationic or anionic), biomolecules,[3] or even a molecule.[2] Here, we report that this method provides a simple yet efficient way to deposit magnetic nanoparticles based on Prussian-blue analogues over nanometric areas, with an accuracy that allows us to place one single nanoparticle on a ~30 nm LON-SiO_2 mark. In this report and compared with the unconventional wet lithography strategy previously used by Coronado *et al.* to pattern magnetic materials,[6] we have been successful in avoiding agglomeration of the nanoparticles and have obtained a very precise nanometric deposition that allowed us to place one single nanoparticle on a ~30 nm LON-SiO_2 mark.

PBA is a family of molecule-based magnetic compounds of general formula $A_xM_y[M'(CN)_6]_z$ (where A is an alkali-metal cation and M and M' are transition metal ions) whose magnetism can be tuned by an external stimulus. Even though the study of PBA has traditionally been limited to bulk compounds, lately they have also been processed onto surfaces as films[7] and more recently into nanoparticles[8] opening the possibility of using them for the development of new electronic or spintronic devices. However, there are still several limitations to overcome in order to accomplish this objetive. For example, in the particular case of NPs they need not only to be deposited on a controllable way, but also to be positioned on specific regions of the surface. So far a major effort has been focused on the deposition of these PBA-NPs.[9] For example Fleury and

Prof. E. Coronado, Dr. A. Forment-Aliaga,
E. Pinilla-Cienfuegos
Instituto Ciencia Molecular (ICMol)
Univ. Valencia,
C/Catedrático José Beltrán 2, E-46980, Paterna, Spain
E-mail: eugenio.coronado@uv.es;
alicia.forment@uv.es
Dr. S. Tatay
Unité Mixte de Physique CNRS/Thales
1 Avenue Augustin Fresnel, F-91120, France
Dr. L. Catala
Institut de Chimie Moléculaire et des Matériaux d'Orsay
CNRS, Université Paris Sud 11, 91405 Orsay, France
Dr. J. A. Plaza
Instituto de Microelectrónica de Barcelona IMB-CNM (CSIC)
Campus UAB-Bellaterra
E-08193, Barcelona, Spain

DOI: 10.1002/adfm.201200067

co-workers have recently managed to graft PBA-NPs on Si(100) by bonding the NPs to a coordination Ni(II) compound previously linked to a SAM on a Si oxide-free surface.[10] In a further step the same group patterned PBA-NPs over large areas of Si(100) surfaces using Focused Ion Beam lithography (FIB).[11] However, these reports, yet pioneering, involve a tedious several step grafting procedure in which micrometic PBA-NPs patterns are produced. To avoid this limitation, an easier protocol leading to deposit PBA-NPs at the nanoscale would be desirable. In this scenario, we have taken advantage of the anionic nature of the PBA-NPs to develop a simple procedure for their nanopatterning. The method uses the electrostatic interactions established between the negatively charged nanoparticles and a SAM of positively charged APTES selectively grown on SiO_2 marks created through LON. Moreover, the evolution of the height of LON-SiO_2 marks during all the procedure has been studied for the first time.

2. Results and Discussion

2.1. Deposition Experiments

For this study we chose $A_xNi[Cr(CN)_6]_y$ (A = Cs, K) bimetallic cyanide-bridged coordination nanoparticles.[8c] These NPs are stable in aqueous solution at pH = 6-7 and show superparamagnetic behavior with blocking temperatures (T_B) above 4 K.[10,12] When Cs^+ was used as counteranion the size of the NPs was estimated to be approx. 6 nm as calculated from dynamic light scattering (DLS) (Figure S1.a) and AFM measurements. To complete the study, higher diameter $K_xNi[Cr(CN)_6]_y$ nanoparticles were also used (approx. 25 nm from DLS (Figure S1.b) and AFM measurements). The only difference in this case is the cation, which compensates the charge of the PBA structure (K^+ instead of Cs^+) and the associated difference in the size of the NPs. Before performing the LON patterning, an exhaustive study about the affinities of the PBA-NPs was carried out on two types of SAMs: APTES and octadecyltrichlorosilane (OTS), and on two types of surfaces: native SiO_2 and nanolithographically oxidized surfaces (LON-SiO_2 surfaces). In a typical experiment the different surfaces were prepared according to the procedure described in the Experimental Section. Briefly, the substrates were sonicated in a pH = 1 aqueous solution for 7 minutes and dried under N_2 without rinsing. The NPs were then deposited during 1 minute over the substrates by drop casting 50 µL of a freshly prepared 1 mM in Ni aqueous PBA-NPs solution. Next the substrates were rinsed with water and dried under a N_2 stream. Finally, the number of deposited nanoparticles was studied by AFM. The obtained results are shown in **Figure 1**.

One observes that PBA-NPs scarcely attach over silicon substrates covered either with native SiO_2, LON-SiO_2 or OTS. However, functionalization of native SiO_2 or LON-SiO_2 marks with APTES largely increases the number of deposited NPs. That can be explained in terms of electrostatic interactions. While in the case of SiO_2 and OTS no protonation is expected at low pH, the $-NH_2$ group in the APTES SAM at pH = 1 will get protonated, at least to some extent.[13] So, the surface will be positively charged attracting the negatively charged PBA-NPs. These nanoparticles remain attached at the surface even after sonication in water for some minutes. This result shows the strong electrostatic attachment of the NPs with the APTES in spite of the lack of covalent bonds. Notice that this electrostatic interaction can be very useful in order to maintain physical properties of the particles unmodified.

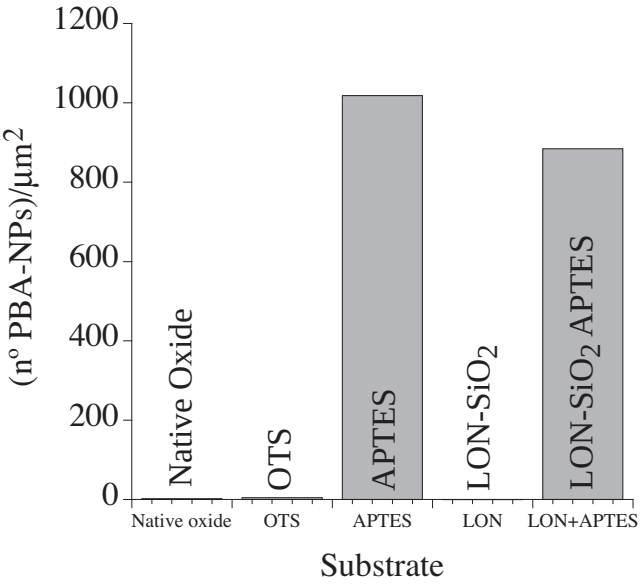

Figure 1. Columns graphic about the number of $Cs_{0.7}Ni[Cr(CN)_6]_{0.9}$ NPs per square micrometer adhered onto different surfaces: Native oxide (SiO_2), OTS, APTES, LON-SiO_2 mark, and LON-SiO_2+APTES functionalized surface. All the surfaces were treated in diluted HCl solution (7 minutes sonication) before PBA-NPs deposition.

In the case of PBA-NPs the strength of the interaction between the surface and the NPs cannot be freely modified by changing the pH of the NPs solution as we did before for the positioning of ferritine biomolecules,[3] nor it is possible to change too much their concentration, as this will compromise the integrity of the NPs, which are based on coordination compounds. However, it was possible to modulate the strength of the interaction by controlling the time during which APTES substrates were sonicated in a pH = 1 aqueous solution before getting in contact with the PBA-NPs. In this approach the pH of the PBA-NPs solution was not modified, but the substrates were immersed in acidic aqueous solutions to enhance the protonation of the amino groups of the APTES layer as that maximizes electrostatic interactions during the deposition step.[13] With sonication times equal or higher than 7 minutes, a particle density as high as 940–1100 NP/µm^2 was always obtained, whereas with sonication times below 7 minutes the density of particles decreased and the method became not reproducible. The fact that sonication, instead of merely immersion in the acid solution, yielded better results can be explained by the presence of a relatively high amino density in an hydrophobic environment which arises from a disordered structure that exposes methylene groups at the surface, as previously described by others.[14] Once a surface amine group is exposed, it is protonated and its positive charge can suppress the protonation of neighboring groups. Moreover, poor solvation and bridging between neighboring charged groups would also suppress

further protonation. In this scenario, the sonication will help to overcome the kinetic reorganizations barriers speeding up the protonation process.[13] Together with the sonication effect an increase in temperature during the process could be responsible of the changes observed, however the monitorization of the temperature in the sonication bath indicates that after 7 minutes of sonication, there is no change in temperature. Only after long sonication periods (>15 min., see Experimental Section) the observed increase in sonication bath temperature could contribute to further speed the protonation process.

2.2. Chemical and Physical Characterization of the Grafted PBA-NPs

To get a chemical characterization of the samples, we complemented the AFM measurements with spectroscopic studies. Attenuated total reflection infrared spectroscopy (ATR-IRRAS) of the APTES functionalized SiO_2 substrates fully covered with PBA-NPs were carried out to confirm the presence of the NPs. The spectrum shows the characteristic 2171 cm^{-1} peak associated with the existence of bridging CN groups in the PBA-NP framework (**Figure 2**).[11] For proving the chemical composition of the surfaces, we complementarily performed AES measurements[15] on two kinds of samples: Sample 1 formed by a silicon substrate coated with APTES (Figure S2.a), and Sample 2 formed by PBA-NPs grafted on a silicon substrate coated with APTES (Figure S2.b). Measurements performed on Sample 1 evidence the presence of the SAM of APTES over the SiO_2 substrate (Si 95 eV, C 274 eV and O 473, 490, 512 eV peaks). In Sample 2, both the additional detection of Ni (717, 783, 851 eV), Cr (531 eV) and Cs (562, 574 eV) peaks along with an increased amount of C (272 eV) and N (385 eV), derived from the presence of the CN groups, clearly evidence the presence of the PBA-NPs.[16]

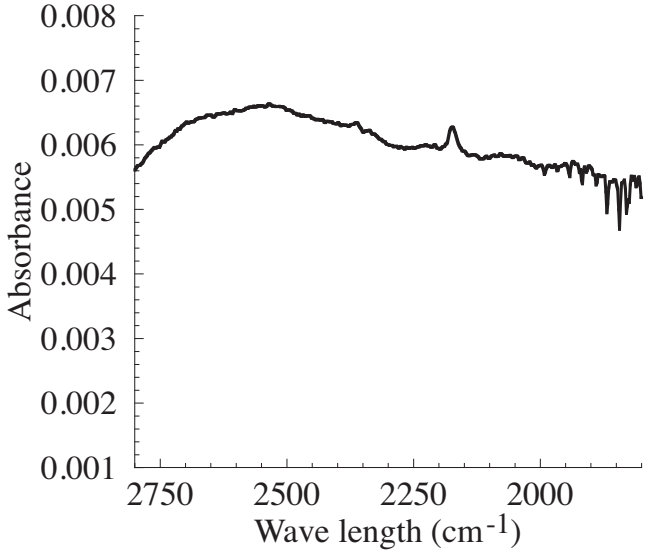

Figure 2. ATR-IRRAS of the $Cs_{0.7}Ni[Cr(CN)_6]_{0.9}$ NPs grafted on a APTES functionalized silicon substrate. Substrate was sonicated at pH = 1 before NPs deposition.

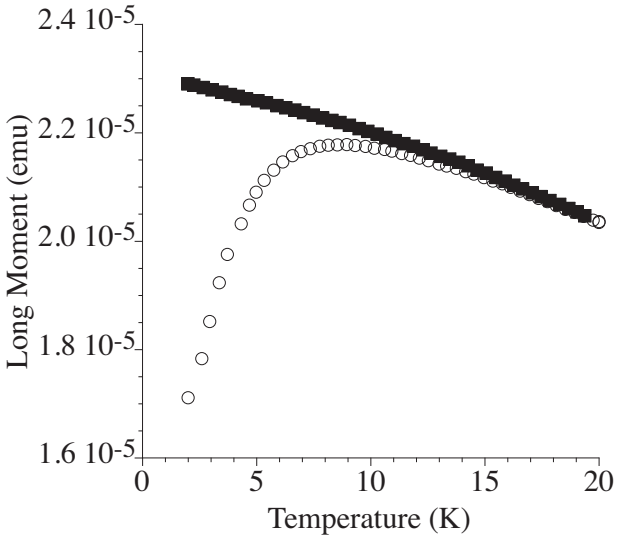

Figure 3. ZFC (empty circles) and FC (full squares) magnetization measurements for the $Cs_{0.7}[NiCr(CN)_6]_{0.9}$ nanoparticles grafted on a silicon wafer previously functionalized with a protonated APTES monolayer.

Magnetic properties of the deposited nanoparticles were studied using a SQUID magnetometer. In order to overcome the problem of the low amount of magnetic sample (a submonolayer of PBA-NPs) on a large amount of diamagnetic material (silicon wafer with an APTES monolayer) a setup similar to the one proposed by B. Fleury et al.[10] was prepared (see Experimental Section). In this setup, the contribution to the overall signal of the silicon wafer is minimized during the measurement and only the magnetic signal from the PBA-NPs is directly recorded. Field-cooled (FC) and Zero-field-cooled (ZFC) magnetization measurements were performed under 100 Oe applied magnetic field. As can be seen in **Figure 3** the two curves diverge below T = 14 K and the maximum of the ZFC is observed at 9 K (slightly higher than the NPs blocking temperature in a polymer matrix and in alternate NiFe (paramagnetic)–NiCr (ferromagnetic) ultrathin films).[10,12,17] This blocking temperature corresponds to magnetically nearly isolated particles. Notice that the high NPs density on the surface prevents the completely isolated behavior. This limitation could be easily overcome by preparing samples with lower density PBA-NPs on the surface (for example by decreasing the protonation ratio of APTES monolayer or by lowering the deposition times). Still, the resulting decrease in the amount of magnetic material will sharply reduce signal intensity and will make the experimental measurements very difficult to perform.

2.3. Patterning Experiments

2.3.1. Procedure

By combining the LON with the functionalization of SiO_2 with SAMs of OTS and APTES, we were able to position PBA-NPs with nanometric precision over Si surfaces. **Scheme 1** shows the protocol. First, silicon wafers were freshly cleaned in H_2O_2:NH_4OH:H_2O (1:1:2) solution. Next, they were

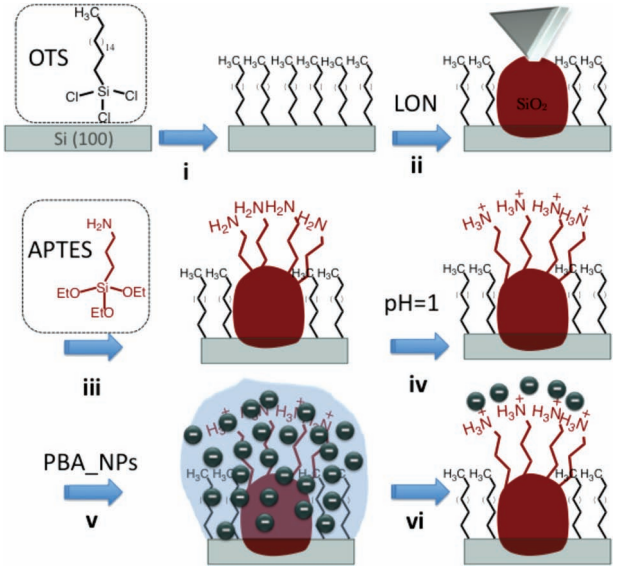

Scheme 1. Steps: i) OTS monolayer formation, ii) LON pattern by means of a specific applied voltage, iii) APTES monolayer formation on top of the bare LON pattern, iv) immersion and sonication of the sample in pH = 1 aqueous solution, v) deposition of PBA-NPs by drop casting the solution on top of the substrate and vi) last sample is rinsed with water and dried under a N_2 stream.

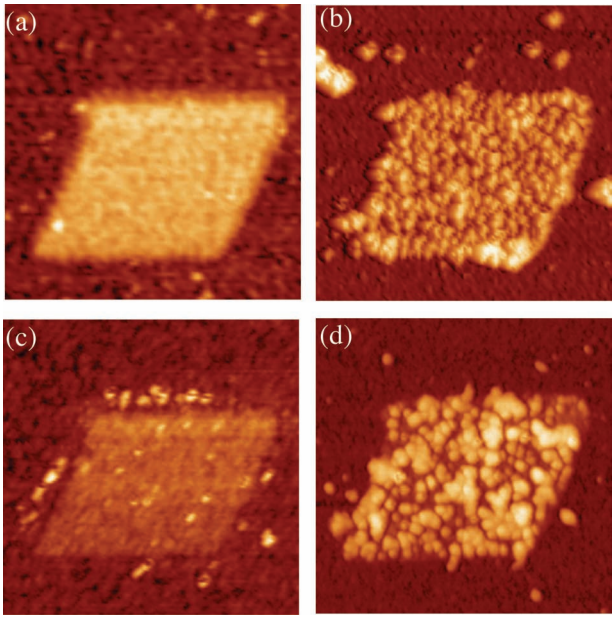

Figure 4. AFM topography images (660 nm x 660 nm each one) representation of different steps of the $Cs_{0.7}Ni[Cr(CN)_6]_{0.9}$ NPs deposition process on nanolitographed patterns. (a) OTS-functionalized substrate was patterned by LON and then marks were modified with protonated APTES. (b) PBA-NPs solution was deposited on the substrate and a clear preference for the modified nanolitographed pattern was shown. (c) Deposited NPs were removed by sonication in acid solution. (d) Deposition process was successfully repeated.

functionalized with an OTS monolayer (i). OTS-functionalized substrates were patterned by means of LON with features of different shapes and heights (ii). The patterned substrates were then functionalized with APTES that reacts specifically with the freshly prepared LON-SiO_2 marks (iii). At this point, a good quality OTS monolayer is indispensable to prevent the APTES grafting outside the lithographed zones. After APTES functionalization the substrates were immersed in a diluted pH = 1 acid solution and sonicated for at least 7 min. (iv). During this step, amino groups got protonated and therefore the SiO_2 marks covered with APTES got positively charged. Without rinsing, a ~50 µL drop of a solution 1 mM in Ni of PBA-NPs was deposited on top of the substrate for 1 min. (v); afterwards, the sample was rinsed with Mili-Q water and dried under a N_2 stream (vi). Occasionally, as a last cleaning step, sonication in water for few minutes was required.

Figure 4 shows an APTES-LON modified substrate before (Figure 4a) and after (Figure 4b) NPs deposition. In Figure 4b one can observe the high preferentiality and nanoparticle density obtained during the deposition process. In some rare cases NPs could be removed from the marks by sonication in the same acid solution used to protonate the APTES molecules (Figure 4c). The reason why they were not always removed under these conditions is still unclear for us. In any case, whenever particles were removed from the surface, deposition process could be repeated (Figure 4d).

To further highlight the importance of electrostatic interactions in our grafting protocol (**Figure 5**) in a first experiment an OTS functionalized substrate was patterned with LON-SiO_2 marks (Figure 5a), immersed into ethanol (without APTES molecules), sonicated in aqueous pH = 1 solution and dried under N_2. Then, PBA-NPs were deposited on this substrate by drop casting. In this case, AFM measurements show that a very low number of NPs got attached to the surface either inside or outside the mark (Figure 5b), in full agreement with our previous observation (Figure 1). In a second experiment the same sample was immersed in an APTES solution to functionalize the mark and then sonicated in diluted HCl. Then PBA-NPs deposition was repeated and the mark was imaged again. In this case, the mark appeared covered with NPs (Figure 5c) while the rest of the surface remained free of them. This is a clear proof of the essential role played by APTES during the deposition of PBA-NPs. In spite of the fact that in some cases the precise number of NPs attached to the functionalized oxide mark was very difficult to quantify, the accurate measurements in z direction confirmed that the NPs were not piled up on top of the lithographed patterns.

As discussed in the previous section, electrostatic driving forces seem to control the clear preferential deposition of the negatively charged PBA-NPs on the cationic APTES surface. This preferentiality was achieved regardless of the size of the marks which includes large strips ~400 nm × 400 nm (Figure 5a), lines ~70 nm × 400 nm (Figure 5d) or even dots of less than 75 nm in diameter (Figure 5e). Such a result proves the very precise control achieved on the organization of these negatively charged nanoparticles on surfaces at length scales ranging from hundreds to tens of nanometers.

To demonstrate the possibility of extending this precise electrostatic organization procedure to PBA-NPs of different

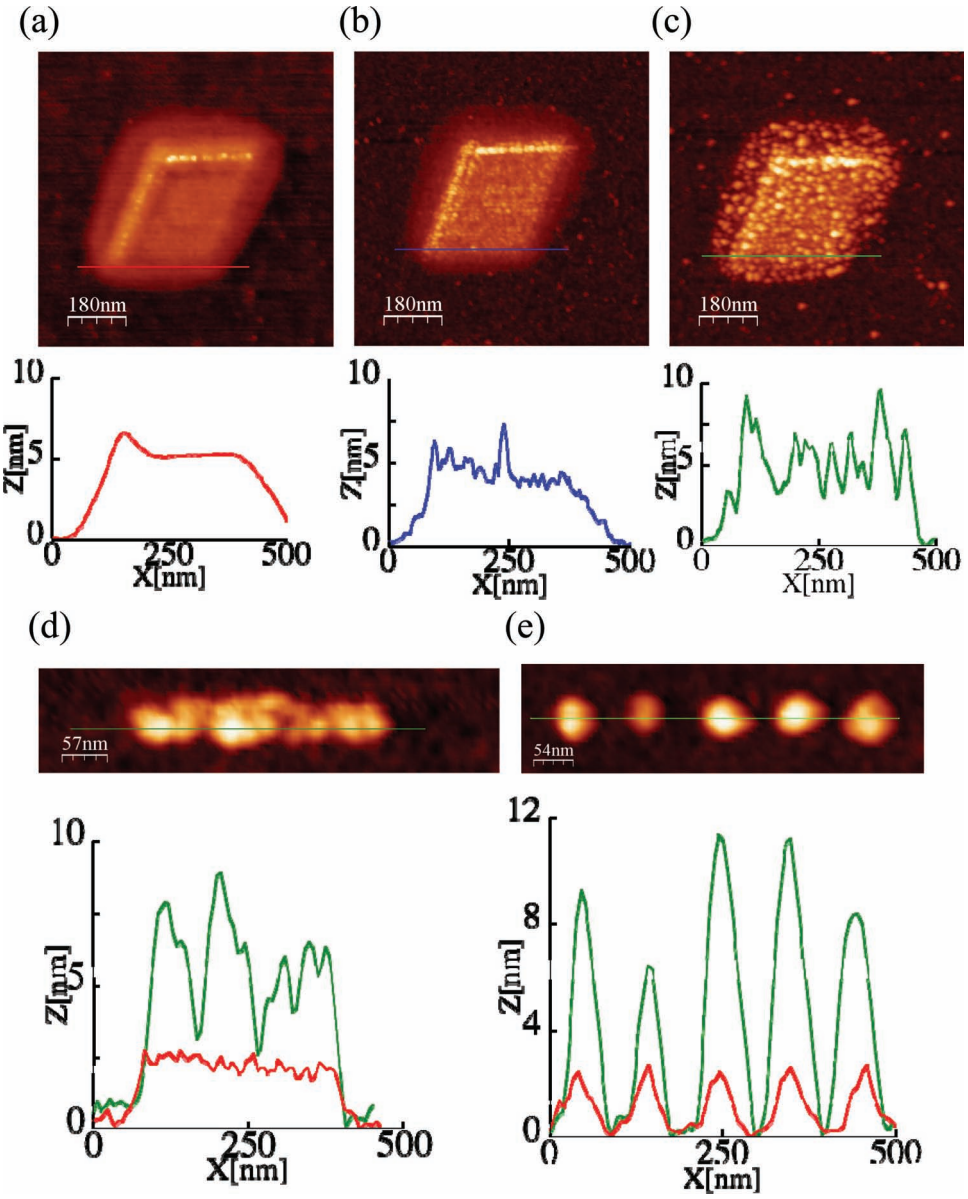

Figure 5. AFM topography images and profiles of: (a) LON-SiO_2 mark patterned on a silicon wafer previously covered with a OTS monolayer (red profile); (b) the same mark after deposition of $Cs_{0.7}Ni[Cr(CN)_6]_{0.9}$ NPs. The substrate was treated with ethanol and diluted HCl but without APTES (blue profile) (see text); (c) the same mark after functionalization with APTES and diluted HCl and deposition of same PBA-NPs (green profile); (d) and (e) deposition experiment on APTES modified LON-SiO_2 marks with different shapes and sizes (red profile: before NPs deposition, green profile: after NPs deposition).

sizes and chemical compositions PBA-NPs $K_xNi[Cr(CN)_6]_y$ of large sizes (approx. 25 nm) were prepared by elimination of the Cs^+ cation from the reaction solution. Next, the same deposition protocol was applied. As can be seen in **Figure 6**, high preferentiality and precision were maintained in this case too. Interestingly, these larger nanoparticles showed a selective preferentiality for the larger marks (**Figure 7**). Such a result was not observed with the smaller 6 nm $Cs_{0.7}Ni[Cr(CN)_6]_{0.9}$ nanoparticles. In this case, single NPs were trapped in marks of about 30 nm width (1.5 nm height) (Figure 7a, 7b). However, the minimum mark size needed to attach a 25 nm NP was larger. In fact, marks of around 100 nm in diameter (3 nm height) were necessary to trap these NPs. Moreover, at least 4 or 5 NPs were usually found on a single mark (Figure 7c). The interdependence between oxide motives size and NPs size, opens the door to the selective deposition of nanoparticles of specific sizes and to the hierarchical organization of NPs of different sizes on the same substrate (Figure S3). A more detailed study about this particular point is already in progress.

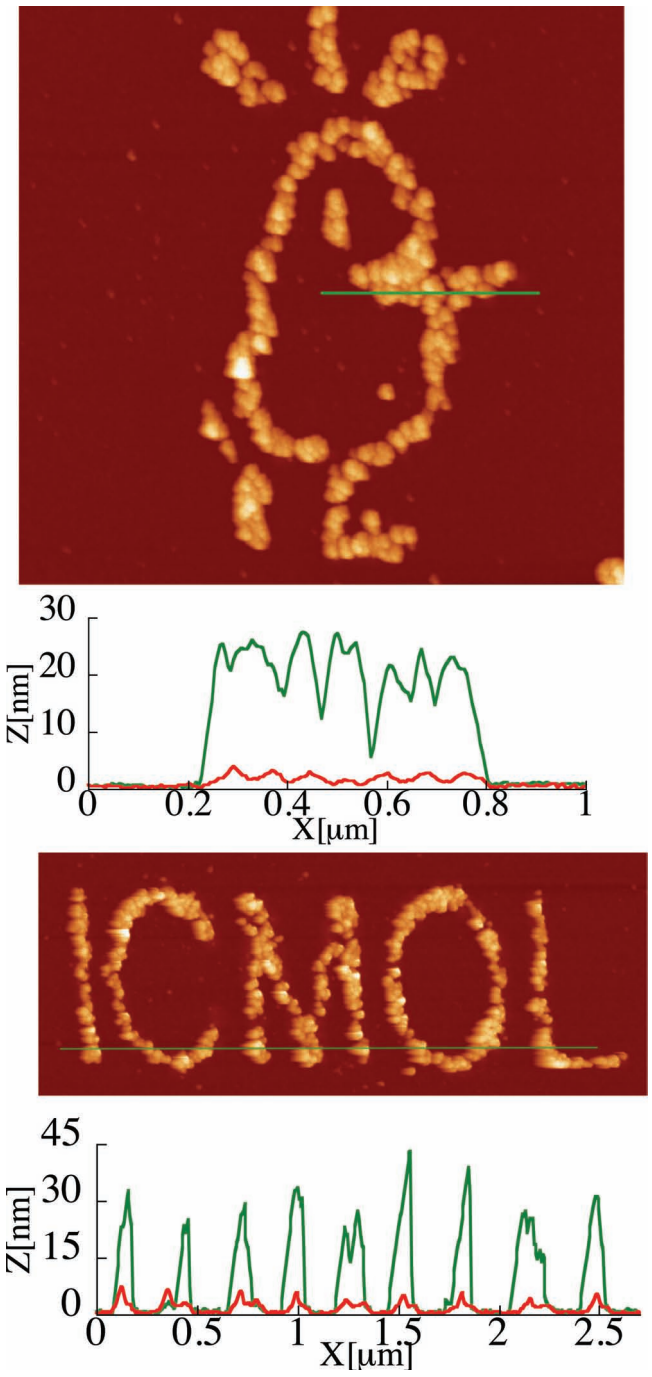

Figure 6. AFM topography images of different nanolithographed patterns on a OTS monolayer with $K_x[NiCr(CN)_6]_y$ nanoparticles on top with their corresponding height profiles (red: before NPs deposition; green: after NPs deposition). Marks were functionalized as ususal with protonated APTES before NPs deposition. (Top image size: 2.7 µm × 2.7 µm; bottom image: 3.1 µm × 1.3 µm).

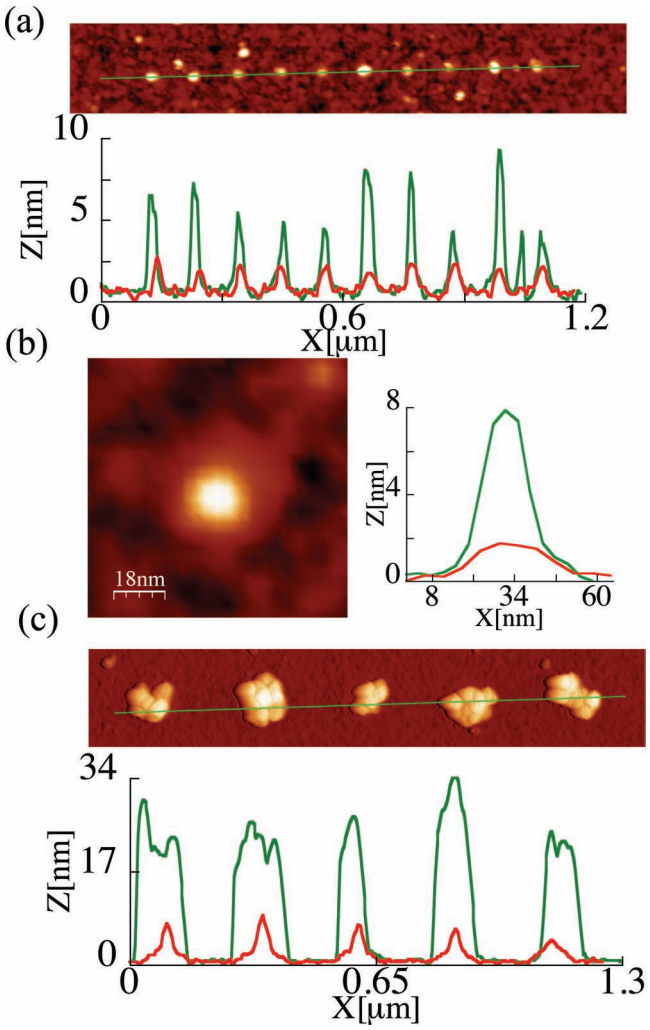

Figure 7. AFM topography images of: (a) $Cs_{0.7}[NiCr(CN)_6]_{0.9}$ nanoparticles (image size: 1.40 µm x 0.23 µm); (b) zoom image and profile of 7th dot in (a) where one single NP has been attached (image size: 90 nm × 90 nm); (c) $K_x[NiCr(CN)_6]_y$ nanoparticles on nanolithographed dots (image size: 1.40 µm x 0.23 µm). Below/next each image, the corresponding superposition of height profiles before (red) and after (green) NPs deposition are shown.

2.3.2. Chemical Characterization of the PBA-NPs Deposited on the Marks

The characterization of PBA-NPs deposited on marks patterned on a silicon wafer covered by an OTS monolayer is a challenge due to the small size of the patterns and the small amount of material to analyze. These limitations make impossible the use of ATR-IRRAS. Instead, the scanning AES technique, that is specially suited to investigations of small surface features, was used for the chemical analysis. This technique provides the possibility to simultaneously produce physical images and element distribution maps of the surface by combining scanning electron microcopy imaging and AES analysis capabilities. We performed AES on top and outside the LON patterns (**Figure 8**). Compared with the experiments on full substrates (section 2.2), longer exposition times and a special care to avoid degradation of the sample were required in this case in order to get enough amount of signal. Inside the LON patterns, apart from the C (275 eV), O (473, 491, 512 eV) and Si (96 eV) peaks coming from the APTES SAM and the substrate, Ni (720, 778, 783, 849 eV), Cs (559, 574 eV), and N (386 eV) Auger peaks

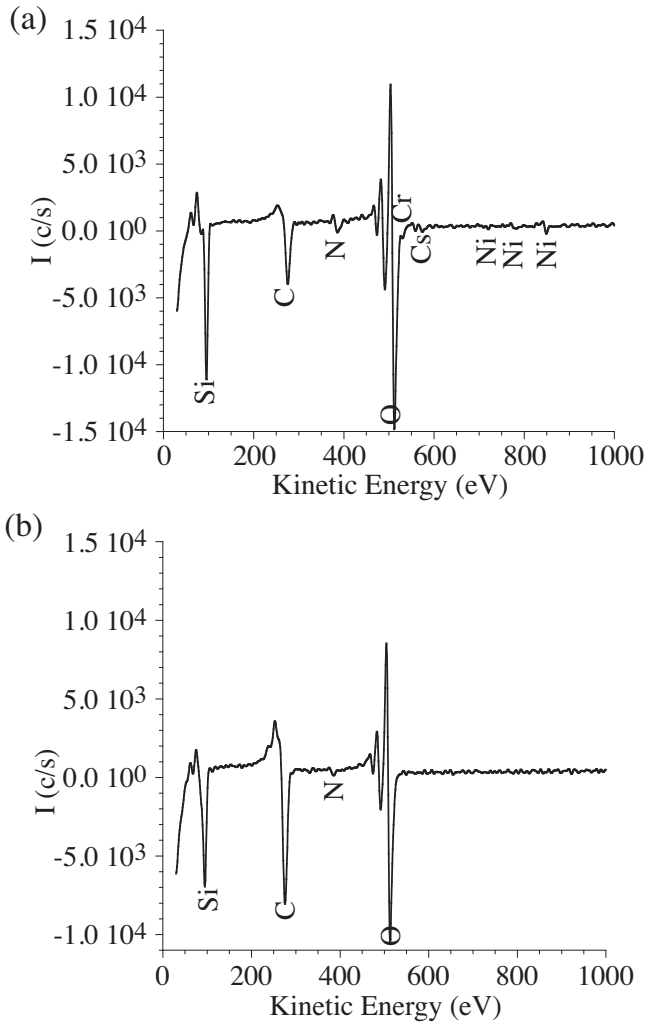

Figure 8. Auger electron spectra of: (a) PBA-NPs on top of a LON-SiO_2 mark modified with protonated APTES; (b) a region of the surface far from the nanolitographed mark. (A table summarizing the most important Auger peaks of the sprectra and the corresponding values found in literature is included in Figure S2).

were detected. This result proves the presence of the PBA-NPs on the functionalized nanopatterned marks (Figure 8a). Outside the marks, the Auger peaks coming from OTS and the substrate were measured (C (276 eV), O (475, 492, 513 eV), and Si (95 eV)). Traces of N (386 eV), but no Ni peaks were also detected (Figure 8b) further proving the preferentiality of our deposition protocol.[16] The presence of N traces could come from some grade of contamination due to the contact with different nitrogen containing impurities in the solvents during sample preparation or to the presence of a small amount of APTES defects inserted in between the SAM of OTS.

2.3.3. Marks Evolution

During our studies we tracked the height profile of the marks in close detail and we realized that it decreased after prolonged sonication. The study of this effect in different solvents and conditions (Figure S4) led us to conclude that although the effect is general, no easy correlation between height decrease and sonication time can be established. But it was clearly observed that a prolonged sonication in acidic solutions produced a decrease in the height of the mark. This fact moved us to progressively reduce sonication times in diluted HCl until a compromise was achieved. Sonicating the samples in diluted HCl for 7 minutes slightly affects the height of the marks while still assures an effective protonation of the APTES monolayer and therefore, high NPs deposition densities (see Section 2.1). A decrease in the height of the mark may wrongly indicate that during the sonication process at pH = 1 the APTES monolayer has been removed along with part of the SiO_2. In this scenario the protonation of the SiO_2 mark and the presence of trapped ionic species[18] would be the ones that induce the electrostatic attachment of the PBA-NPs onto the surface making unnecessary the APTES monolayer. Still, it has been previously shown (section 2.1, Figure 1 and Figure 5) that the presence of APTES is crucial for the attachment of the NPs. From our point of view, we can assume that even if some APTES molecules are removed from the surface during the sonication steps, they may be trapped again in the remaining SiO_2. Moreover, the non-stoichiometric and porous character of the fabricated oxide[18] can favor such a trapping.

3. Conclusions

In summary, we have presented an easy approach for the selective deposition and accurate organization of PBA nanoparticles into very specific positions of a native silicon surface with submicrometric precision. In fact, a single PBA-NP has been anchored onto a LON nanometric mark of SiO_2 for the first time. This method combines a top-down approach (LON) with a bottom-up approach based on the functionalization of a silicon surface with SAMs of neutral OTS and cationic APTES selectively deposited onto the LON-SiO_2 marks. Compared with previous results, the method developed in this work has introduced the following improvements:

i) An increase of the electrostatic interaction through sonication in acid solution of the sample, leading to an enhancement in the protonation of the SAM of APTES, has been achieved. This step is crucial to selectively attach one single nanoparticle on a nanometric LON-SiO_2 mark.
ii) The influence of the combination of applied LON voltage, oxidation time and sonication has been highlighted. The first two parameters are useful in order to control the initial size of the SiO_2 mark,[19] while we have observed that the sonication time is important for the final size of the SiO_2 mark functionalized with APTES. In this context, we have shown that, even after strong sonication the APTES molecules, originally assembled onto the SiO_2 mark, prevail in the marks maintaining their recognition properties.
iii) Thanks to the possibility of tuning nanoparticles diameter we have observed a relevant interdependence between nanoparticles size vs marks size.
iv) The electrostatic nature of the method grants the electronic decoupling from the surface of the PB-NPs, assuring the prevalence of the physical and chemical properties of the

particles as demonstrated by magnetometry, ATR-IRRAS (on NPs monolayer) and AES (on a single mark).

Finally, we would like to emphasize that despite being a serial method, LON in general, and the particular strategy fellow here are compatible with μ-contact printing technologies and can be eventually upscaled.[20–22] In the particular case of PBA-NPs this extension is currently in progress with promising results (Figure S5) and will be published in a future report.

4. Experimental Section

PBA-NPs: A solution of $Cs_{0.7}Ni[Cr(CN)_6]_{0.9}$ nanoparticles was prepared on base of the synthetic procedure previously described by L. Catala *et al.*[8c] 50 mL 2.10^{-3} M aqueous solution of $K_3Cr(CN)_6$ was quickly added to 50 mL of 2.10^{-3} M $NiCl_2.6H_2O$ and 4.10^{-3} M CsCl aqueous solution. The suspension was stirred for at least 1 hour at room temperature before using it. $K_xNi[Cr(CN)_6]_y$ nanoparticles suspension was prepared following exactly the same procedure except for the CsCl salt, that was not included in the reaction mixture.

Substrates: The substrates used for the NPs deposition on LON-SiO_2 marks were silicon wafers (p-type) with a marker code made by means of optical lithography, in this way it was possible to localize exactly the same position on the sample. These substrates were prepared by optical lithography in the Instituto de Microelectrónica de Barcelona. For experiments where localization of specific positions was not required, common silicon wafers (p-type <100> from DXL enterprises, INC) were used.

Cleaning procedure: Silicon wafers with or without photolithographed marked code were cleaned always just before any experiment was performed. Samples were sonicated 10 minutes in freshly prepared H_2O_2:NH_4OH:H_2O (1:1:2) solution three times. Then they were rinsed with mili-Q water, sonicated 5 minutes in mili-Q water twice and dried under a N_2 stream. Substrates with the photolitographed code were briefly sonicated in organic solvents before the cleaning process with the oxidant mixture to assure the elimination of any photoresistor residue.

Ultrasonic cleaner: a BRANASONIC MTH-5510 ultrasonic cleaner (power 185 W) was used. During different experiments we monitorized the temperature of the sonication bath, but no significant change in temperature was observed for sonication times below 15 minutes (approx. +15 min. +1 °C).

SAMs preparation: OTS (90+%), APTES (99%) molecules and solvents were purchased from Aldrich and used without previous purification. Once OTS and APTES bottles were opened, they were kept always under N_2 atmosphere to avoid any degradation. OTS monolayers were prepared inside a glove box. Clean silicon substrates were dipped in 2.8 mM OTS in toluene (puriss, over molecular sieve) and kept in solution for three days, then they were rinsed with toluene and sonicated in toluene, chloroform and 2-propanol to remove any physisorbed material/molecules and dried under N_2 stream. The quality of the SAMs was evaluated by advancing–receding contact angle measurements in a Ramé-hart automatized goniometer and by AFM imaging. APTES SAMs were prepared by dipping the substrates in 1 mM APTES in ethanol (absolute, reagent grade) for 45 minutes, then rinsed with ethanol and sonicated twice in this solvent for 5 minutes. Finally, substrates were dried under N_2 stream. Due to the similar contact angle values between APTES monolayer and clean silicon, these SAMs were only checked by AFM. All glass material used for the SAMs preparation was cleaned with piranha solution (H_2SO_4:H_2O_2, 1:1), rinsed with mili-Q water and sonicated with mili-Q water several times in order to remove any trace of acid and dried in an oven.

AFM measurements and LON: For all the experiments, two different microscopes were utilized, a Nanoscope IIIa AFM (Veeco) with a home-made voltage amplifier for the development of LON and a Nanotec Cervantes Full Mode AFM (Nanotec Electrónica S.L.). Sharp silicon probes without coating (Tapping Mode ~42 N/m, ~320 kHz) were purchased from two different suppliers: TESP probes (Veeco) and PPP-NCH (Nanosensors). Lab humidity was increased by means of a humidifier for household use. All AFM images were processed with WSxM software from Nanotec Electrónica S.L.[23]

PBA-NPs deposition: Nanolitographed patterns were drawn on silicon substrates covered with a good quality OTS monolayer (which removed OTS molecules on the patterned area). The substrates were immersed in 1 mM APTES ethanol solution and all the steps for the growing of an APTES self-assembled monolayer were followed. Next, they were sonicated between 7 and 30 minutes in diluted HCl solution (pH approx. 1). Then the substrates were dried under a N_2 stream and covered with a drop of PBA-NPs solution (1 mM in Ni) (approx. 50 μL) for 1 minute. Afterwards, the nanoparticles solution was removed by rinsing the substrate with mili-Q water and dried with N_2. When a more precise cleaning procedure was needed, the substrates were sonicated in mili-Q water (between 1 and 5 minutes) and dried once more under N_2.

DLS measurements: Size distribution of the NPs samples was determined by DLS of 1 mM in Ni PBA-NPs solution with a Marlvern Zetasizer instrument.

ATR-IRRAS measurements: a VeeMax II sampling stage (Pike Technologies) equipped with a 60° germanium (Ge) ATR crystal and a high-pressure clamp was placed in the sample compartment of a NICOLET 5700 Transformation-Infrared spectrometer. A high-pressure swivel clamp (diameter ~ 7.8 mm) was used to apply even and constant pressure to the sample during FTIR data acquisition. The angle of incident infrared was set ~60° with respect to the surface normal of Ge crystal. Silicon substrates with APTES and a PBA-NPs monolayer film were placed (face down) between the Ge crystal and the tip of the high-pressure clamp. Each FTIR spectrum represents the average of 120 scans at 4 cm^{-1} resolution. A p-polarized infrared beam (by means of a manual polarizer ZnSe) was used and the output signal was collected with a refrigerated MCT/A detector.

AES: The Auger analysis was carried out using a Physical Electronic PHI 680 Auger nanoprobe with a Schottky emission cathode and multi-channel plate detector. The beam voltage acceleration was 10 kV, the beam current 10 nA and the incident angle 30 degrees. For short beam exposition times, these conditions allowed the analysis of single oxide motives without substantial degradation of the organometallic.

Magnetic characterization: Magnetic data were collected with a Quantum Design MPMS XL-5 susceptometer equipped with a SQUID sensor. In order to avoid the diamagnetic contribution of silicon surface, three pieces of Si were introduced in the SQUID measurement cannula. Bottom part: 4 cm × 0.8 cm piece of clean Si, middle: 0.8 cm × 0.8 cm piece of functionalized silicon with a monolayer of PBA-NPs and top: 4 cm × 0.8 cm piece of clean Si. DC Field-cooled and Zero-field-cooled magnetization measurements were performed under 100 Oe applied magnetic field.

Supporting Information

Supporting Information is available from the Wiley Online Library or from the author.

Acknowledgements

Financial support from the European Union (Project ELFOS and ERC Advanced Grant SPINMOL to EC), the Spanish MINECO (Project Consolider-Ingenio in Molecular Nanoscience, CSD2007-00010, and grants MAT2007-61584 and MAT2011-22785, CTQ-2008-06720-C02-01/BQU and GICSERV5) and the Generalitat Valenciana (PROMETEO Program) is gratefully acknowledged. The authors also thank E. Tormos, S. Benmansour, A. López-Múñoz, J. M. Martínez-Agudo, R. V. Martínez and F. Wyczisk for their technical support and F. Volatron for scientific discussion. A.F.-A. thanks the Spanish MINECO for a Ramón y Cajal

contract. S.T wants to thank NANOCON (FP7/2007-2013-252757) project for its financial support.

Received: January 10, 2012
Published online: May 23, 2012

[1] M. Cavallini, F. C. Simeone, F. Borgatti, C. Albonetti, V. Morandi, C. Sangregorio, C. Innocenti, F. Pineider, E. Annese, G. Panaccione, L. Pasquali, *Nanoscale* **2010**, *2*, 2069–2072.

[2] R. V. Martínez, F. García, R. García, E. Coronado, A. Forment-Aliaga, F. M. Romero, S. Tatay, *Adv. Mater.* **2007**, *19*, 291–295.

[3] a) R. V. Martínez, J. Martínez, M. Chiesa, R. García, E. Coronado, E. Pinilla-Cienfuegos, S. Tatay, *Adv. Mater.* **2010**, *22*, 588–591; b) T. Yoshinobu, J. Suzuki, H. Kurooka, W. C. Moon, H. Iwasaki, *Electrochim. Acta* **2003**, *48*, 3131–3135.

[4] J. Zheng, Z. Zhu, H. Chen, Z. Liu, *Langmuir* **2000**, *16*, 4409–4412.

[5] a) S. Hoeppener, R. Maoz, S. R. Coen, L. Chi, H. Fuchs, J. Sagiv, *Adv. Mater*. **2002**, *14*, 1036-1041; b) S. Liu, R. Maoz, J. Sagiv, *Nano Lett.* **2004**, *4*, 845–851

[6] E. Coronado, C. Martín-Gastaldo, J. R. Galán-Mascarós, M. Cavallini, *J. Am. Chem. Soc.* **2010**, *132*, 5456–5468.

[7] a) J. T. Culp, J.-H. Park, F. Frye, Y.-D. Huh, M. W. Meisel, D. R. Talham, *Coord. Chem. Rev.* **2005**, *249*, 2642–2648; b) S. Lepoutre, D. Grosso, C. Sanchez, G. Fornasieri, E. Rivière, A. Bleuzen, *Adv. Mater.* **2010**, *22*, 3992–3996.

[8] a) S. Vaucher, M. Li, S. Mann, *Angew. Chem.* **2000**, *112*, 1863–1866; *Angew. Chem. Int. Ed.* **2000**, *39*, 1793–1796; b) S. Vaucher, J. Fielden, M. Li, E. Durjardin, S. Mann, *Nano Lett.* **2002**, *2*, 225–229; c) D. Brinzei, L. Catala, N. Louvain, G. Rogez, O. Stéphan, A. Gloter, T. Mallah, *J. Mater. Chem.* **2006**, *16*, 2593–2599; d) L. Catala, T. Gacoin, J.-P. Boilot, É. Rivière, C. Paulsen, E. Lhotel, T. Mallah, *Adv. Mater.* **2003**, *15*, 10, 826–829; e) L. Catala, F. Volatron, D. Brinzei, T. Mallah, *Inorg. Chem.* **2009**, *48*, 3360–3370 and references therein; f) G. Clavel, J. Larionova, Y. Guari, C. Guerin, *Chem.–Eur. J.* **2006**, *12*, 3798–3804; g) Y. Guari, J. Larionova, K. Molvinger, B. Folch, C. Guerin, *Chem. Commun.* **2006**, 2613–2615; h) L. Catala, D. Brinzei, Y. Prado A. Gloter, O. Stéphan, G. Rogez, T. Mallah, *Angew. Chem.* **2008**, *121*, 189–193; *Angew. Chem. Int. Ed.* **2009**, *48*, 183–187.

[9] M. Clemente-León, E. Coronado, Á. López-Muñoz, D. Repetto, C. Mingotaud, D. Brinzei, L. Catala, T. Mallah, *Chem. Mater.* **2008**, *20*, 4642–4652.

[10] B. Fleury, F. Volantron, L. Catala, D. Brinzei, E. Rivière, V. Huc, C. David, F. Miserque, G. Rogez, L. Baraton, S. Palacin, T. Mallah, *Inorg. Chem.* **2008**, *47*, 1898–1900.

[11] A. Ghirri, A. Candini, M. Evangelisti, G.-C. Gazzadi, F. Volatron, B. Fleury, L. Catala, C. David, T. Mallah, M. Affronte, *Small* **2008**, *12*, 2240–2246.

[12] Y. Prado, L. Lisnard, D. Heurtaux, G. Rogez, A. Gloter, O. Stéphan, N. Dia, E. Rivière, L. Catala, T. Mallah, *Chem. Commun.* **2011**, *47*, 1051–1053.

[13] J.-J. Shyue, M. R. De Guire, T. Nakanishi, Y. Masuda, K. Koumoto, C. N. Sukenik, *Langmuir* **2004**, *20*, 8693–8698.

[14] a) M. L. Wallwork, D. A. Smith, J. Zhang, J. Kirkham, C. Robinson, *Langmuir* **2001**, *17*, 1126–1131; b) D. V. Vezenov, A. Noy, L. F. Rozsnyai, C. M. Lieber, *J. Am. Chem. Soc.* **1997**, *119*, 2006–2015; c) E. W. Van Der Vegte, G. Hadziioannou, *J. Phys. Chem. B* **1997**, *101*, 9563–9569.

[15] Wilson, *Comprehensive Analytical Chemistry, Non-Destructive micro-analysis of cultural heritage materials*, Vol. *XLII* (Eds: K. Janssens, R. Van Grieken) Elsevier, Belgium **2004**.

[16] K. D Childs, B. A. Carlson, L. A. LaVanier, J. F. Moulder, D. F. Paul, W. F. Stickle, D. G. Watson, *Handbook of Auger Electron Spectroscopy*. 3rd edition, (Ed: C. L. Hedberg) Physical Electronics, USA **1995**.

[17] S. Tricard, C. Costa-Coquelard, S. Mazerat, E. Rivière, V. Huc, C. David, F. Miserque, P. Jegou, S. Palacin, T. Mallah *Dalton Trans.* **2012**, *41*, 4445–4450.

[18] J. A. Dagata, T. Inoue, J. Itoh, K. Matsumoto, H. Yokoyama, *J. Appl. Phys.* **1998**, *84*, 6891–6900.

[19] a) R. García, M. Calleja, F. Pérez-Murano, *Appl. Phys. Let.* **1998**, *72*, 2295–2297; b) R. García, R. V. Martínez, J. Martínez, *Chem. Soc. Rev*. **2006**, *35*, 29–38.

[20] a) F. C. Simeone, C. Albonetti, M. Cavallin, *J. Phys. Chem. C* **2009**, *113*, 18987–18994; b) C. Albonetti, J. Martinez, N. S. Losilla, P. Greco, M. Cavallini, F. Borgatti, M. Montecchi, L. Pasquali, R. Garcia, F. Biscarini, *Nanotechnology* **2008**, *19*, 435303.

[21] M. Cavallini, F. Biscarini *Nano Lett.* **2003**, *3*, 1269–1271.

[22] R. V. Martínez, M. Chiesa, R. García, *Small* **2011**, *7*, 2914–2920.

[23] I. Horcas, R. Fernández, J. M. Gómez-Rodríguez, J. Colchero, J. Gómez-Herrero, A. M. Baro, *Rev. Sci. Instrum.* **2007**, *78*, 013705.